Medical & Biological Engineering & Computing (2023) 61:3363–3385
https://doi.org/10.1007/s11517-023-02843-w

ORIGINAL ARTICLE

Automated diagnosis of EEG abnormalities with different classification techniques

Essam Abdellatef[1] · Heba M. Emara[2] · Mohamed R. Shoaib[3] · Fatma E. Ibrahim[2] · Mohamed Elwekeil[2] · Walid El-Shafai[2,4] · Taha E. Taha[2] · Adel S. El-Fishawy[2] · El-Sayed M. El-Rabaie[2] · Ibrahim M. Eldokany[2] · Fathi E. Abd El-Samie[2,5]

Received: 15 September 2022 / Accepted: 23 April 2023 / Published online: 6 September 2023

Abstract
Automatic seizure detection and prediction using clinical Electroencephalograms (EEGs) are challenging tasks due to factors such as low Signal-to-Noise Ratios (SNRs), high variance in epileptic seizures among patients, and limited clinical data constraints. To overcome these challenges, this paper presents two approaches for EEG signal classification. One of these approaches depends on Machine Learning (ML) tools. The used features are different types of entropy, higher-order statistics, and sub-band energies in the Hilbert Marginal Spectrum (HMS) domain. The classification is performed using Support Vector Machine (SVM), Logistic Regression (LR), and K-Nearest Neighbor (KNN) classifiers. Both seizure detection and prediction scenarios are considered. The second approach depends on spectrograms of EEG signal segments and a Convolutional Neural Network (CNN)-based residual learning model. We use 10000 spectrogram images for each class. In this approach, it is possible to perform both seizure detection and prediction in addition to a 3-state classification scenario. Both approaches are evaluated on the Children's Hospital Boston and the Massachusetts Institute of Technology (CHB-MIT) dataset, which contains 24 EEG recordings for 6 males and 18 females. The results obtained for the HMS-based model showed an accuracy of 100%. The CNN-based model achieved accuracies of 97.66%, 95.59%, and 94.51% for Seizure (S) versus Pre-Seizure (PS), Non-Seizure (NS) versus S, and NS versus S versus PS classes, respectively. These results demonstrate that the proposed approaches can be effectively used for seizure detection and prediction. They outperform the state-of-the-art techniques for automatic seizure detection and prediction.

Keywords Epilepsy · EEG · EMD · Seizure prediction · Seizure detection · HMS

1 Introduction

Epilepsy is a neurological disease that is not contagious, not a mental illness, and not a developmental disability. A seizure is a brief disruption of the electrical activities in the human brain [1]. Epileptic seizures are attributed to deformities in the human brain that make the patient prone to seizures, which are usually frequent and recurrent [2]. According to the International League Against Epilepsy (ILAE), the most recent definition is that "Epilepsy is a disorder of the brain characterized by an enduring predisposition to generate epileptic seizures". This definition of epilepsy requires the occurrence of at least one epileptic seizure. The seizures occur because of sudden and abnormal electrical activities in the brain, or excessive electrical discharges in a group of brain cells. Different parts of the brain can be the source of such discharges. When the nerve cells send distorted signals, they ignite patients with distressed feelings making them act strangely, usually as a spasm or a violent vibration involving the muscles [3–6].

Research studies provided by the World Health Organization (WHO) show that approximately 50 million people suffer from epilepsy worldwide. The estimated proportion of the general population with active epilepsy, i.e., continuing seizures or with the need for treatment at a given time,

✉ Walid El-Shafai
eng.waled.elshafai@gmail.com

Extended author information available on the last page of the article

is between 4 and 10 per 1000 persons [7]. However, some studies in low- and middle-income countries reveal that the proportion is much higher, between 7 and 14 per 1000 persons. Most seizures last from 30 seconds to 2 minutes and do not cause lasting harm [8]. However, there is a medical emergency if seizures last longer than 5 minutes or if a person has many seizures and does not wake up between them. Seizures may start at any time during life and occur sporadically at infrequent intervals or frequently.

EEG is the recording of electrical activities along the scalp produced by the discharging of neurons within the brain. It refers to the recording of the brain spontaneous electrical activities over a period. When brain cells (neurons) are activated, local current flows are produced. The electrical activities are detected using small, and flat metal discs (electrodes) attached to the brain scalp. The brain cells send electrical impulses that are active all the time, even during human sleeping [9].

Automatic seizure detection and prediction from EEG signals have received considerable research attention for a better understanding of epilepsy and more efficient management of the disease. Feature extraction is a key step in performing EEG signal classification for detection or prediction [10]. We imagine courageously a method in which classification is carried out without complex feature extraction, and the recent development of CNN has provided a new way of addressing this issue. Original EEG signals converted to images using spectrogram estimation are directly used to train a CNN. We not only consider binary epilepsy scenarios, e.g., NS versus S and NS versus PS, but also verify the ability to classify NS versus S versus PS.

In this paper, two approaches for detecting and predicting epileptic seizures in EEG signals are introduced. The first one is based on feature extraction in the HMS domain. EEG signals are first split into Intrinsic Mode Functions (IMFs). The instantaneous frequency spectrum of each of the collected IMFs is then obtained using the Hilbert transform. For IMFs, main features such as spectral entropy, skewness, kurtosis, and sub-band energies are extracted and then used. SVM, LR, and KNN are the three classifiers utilized. Secondly, an efficient approach for activity detection from EEG signals is proposed. It incorporates the generation of spectrograms of EEG signals. A CNN is used for the classification of spectrogram images. The proposed model depends on the use of residual learning and depth concatenation techniques. The main contributions of this work can be listed as follows:

– Proposal of an approach that depends on HMS domain and SVM for seizure detection and seizure prediction.
– Proposal of an approach that generates spectrograms of EEG signals and performs various classification scenarios for seizure detection and prediction.
– Proposal of a CNN model to be used for classification. The proposed model incorporates depth concatenation and residual learning strategies.
– Study of the impact of different CNN hyper-parameters on the classification performance.
– Measurement of the performance of the proposed models and comparison with different state-of-the-art models.

2 Related work

In recent years, there has been a growing interest in the utilization of ML and Deep Learning (DL) models for the classification of biomedical data. These models have been applied on a wide range of data types, including EEG signals, Magnetic Resonance Imaging (MRI) scans [11, 12], and electrocardiography (ECG) signals. Various ML and DL techniques, such as SVMs, kNNs, Random Forests (RFs), CNNs, and Recurrent Neural Networks (RNNs), have been used to classify biomedical data with high accuracy and precision. Additionally, several studies have used ensemble methods, such as boosting and bagging, to improve the classification performance. Overall, the use of ML and DL models for the classification of biomedical data is a promising area of research with the potential to revolutionize the field of healthcare [13, 14]. For epileptic seizure detection using EEG signals, many strategies have been developed. In [15], the researchers suggested an automated seizure detection approach in the Empirical Mode Decomposition (EMD) domain. Higher-order statistics, including variance, kurtosis, and skewness, are extracted and utilized as features. An artificial neural network is used for the classification task. Bizopoulos et al. [16] presented HMS analysis in combination with k-means clustering to detect epileptic seizures. The authors of [17] employed a method for detecting seizures from EEG signals based on HMS. As discriminative features, spectral entropies and sub-band energies are utilized. An SVM is used for classification. Ibrahim et al. [18] introduced three models for the classification task of EEG signals. Two of the models are patient-specific and designed for the classification of NS versus PS activities for seizure prediction, and NS versus S activities for seizure detection. The third model is patient non-specific, making it better suited for general classification tasks. The first model utilizes a CNN with residual blocks, containing thirteen layers and four residual learning blocks. It works on spectrograms of EEG signal segments. The second model depends also on a CNN with three layers and works on spectrograms. The third model, in contrast, depends on Phase Space Reconstruction (PSR) to eliminate the limitations of spectrograms used in the first two models. A five-layer CNN is used with this strategy.

Riaz et al. [19] presented a technique for extracting features from EEG signals using the EMD. It depends on temporal moments of the third order, as well as spectral features like the spectral centroid, coefficient of variation, and spectral skewness of the IMFs. These features are physiologically meaningful as they can differentiate normal EEG signals from pathological EEG signals in terms of temporal and spectral centroids, dispersions, and symmetries. The extracted features are then fed into an SVM classifier. For epileptic seizure detection, Hassan et al. [20] employed Complete Ensemble Empirical Mode Decomposition with Adaptive Noise (CEEMDAN). Once the EEG signal segments have been decomposed into CEEMDAN IMFs, these IMFs are modeled using the symmetric Normal Inverse Gaussian (NIG) Probability Density Function (PDF). The estimated NIG parameters are then used as features for the epileptic seizure detection algorithm. The symmetric NIG PDF is a variance-mean mixed density in which the inverse Gaussian density constitutes the mixed distribution. The scale and feature factors of the NIG PDF computed from each of the CEEMDAN IMFs are utilized as features in the epileptic seizure detection algorithm. Bouaziz et al. [21] have managed to segment the EEG signals of CHB-MIT into 2-second frames, and then transformed them into a spatial representation by producing a set of intensity images. These images were fed to a CNN, which has a total of eight layers comprising one initial input layer, five hidden layers, one fully-connected layer, and an output layer. Their approach achieved an accuracy of 99.48%. It managed to reduce dimensionality, and then allow the Genetic Algorithm (GA) classification.

Rajaguru et al. [22] adopted Multilayer Auto-Encoders (MAEs) and Expectation-Maximization merged with Principal Component Analysis (EM-PCA). The performance index represented in classification accuracy was 93.78%. Natural and abnormal brain activities were studied by Roy et al. [23], as they proposed four different DL schemes. The development of the ChronoNet model was conducted based on other models. This model gave 90.60% and 86.57% training and testing accuracies, respectively. A multi-scale 3D-CNN with a bidirectional Gated Recurrent Unit (GRU) model was introduced by Choi et al. [24] for cross-patient seizure detection. Short-Time Fourier Transform (STFT) was used to get spectral and temporal features from EEG signals.

Any proposed method should be able to distinguish between NS and S states, when it comes to seizure detection. Shoeb [25] employed an SVM classifier to identify seizures. His approach achieved a False-Positive Rate (FPR) of 0.08 /h and an average accuracy of 96%. Thodoroff et al. [26] presented a seizure detection approach based on a recurrent convolutional neural network and an image-based EEG signal representation. The results showed a sensitivity of 96% and an FPR of 0.08 /h. In [27], the authors used a hybrid method to select IMFs extracted by EMD and Ensemble Empirical Mode Decomposition (EEMD). For classification, an SVM is utilized. By using EMD and the EEMD, average accuracies of 94.56% and 96.06%, respectively, have been achieved. Truong et al. [28] used the Freiburghigher-order statistic spital intracranial EEG (iEEG) dataset, the CHB-MIT dataset, and the American Epilepsy Society (AES) Seizure Prediction Challenge dataset. To construct spectrograms, the STFT algorithm has been applied to raw data. This patient-oriented model gave sensitivity values of 81.4%, 81.2%, and 75% and FPR values of 0.06/h, 0.16/h, and 0.21/h, for the pre-mentioned datasets, respectively.

For seizure prediction, the Hilbert-Huang Transform (HHT) and a Bayesian classifier were utilized in [29]. First, signals are pre-processed for noise reduction. The HHT is then used to extract features. For feature selection, a Correlation-based Feature Selection (CFS) method was used. For classification, Bayesian networks were utilized. Finally, post-classification, a post-processing technique, was used to merge the individual probabilities gained. This approach has a sensitivity of 96.55% and an FPR of 0.21/h. Consul et al. [30] introduced a Hilbert domain hardware prediction algorithm. After obtaining the instantaneous phase using the Hilbert transform, the Phase-Difference (PD) approach has been used. This approach achieved a prediction time ranging from 51 seconds to 188 minutes and a sensitivity of 88.2%.

Chu et al. [31] used an attractor state-analysis-based seizure predictive model. The accuracy of this model was 86.6%, with a false prediction rate of 0.367/h and an average prediction time of 45.3 minutes. Sedik et al. [32] used a statistical framework based on the use of various digital filters to predict seizures. A prediction time of 66.6 minutes, an accuracy of 96.2485%, and a false-alarm rate of 0.10526/h have been achieved. Emara et al. [33] presented an automatic seizure detection approach based on Scale-Invariant Feature Transform (SIFT) in the frequency domain as a feature extraction tool. This approach has been tested on the CHB-MIT dataset. An accuracy of 99.97% has been achieved. Emara et al. [34] proposed an approach for EEG seizure prediction and channel selection in the Hilbert domain. Signal attributes in the Hilbert domain, including amplitude, derivative, local mean, local variance, and median, are analyzed statistically to perform the channel selection and seizure prediction tasks. An average prediction rate of 96.46%, an average false-alarm rate of 0.028/h, and an average prediction time of 60.16 min for a 90-min prediction horizon have been reported.

Yoo et al. [35] proposed another time-domain detection technique, where the signal energy is computed during S and NS intervals on patient-specific data. They used SVM as a classifier with an accuracy of 84.4%. In addition, there are several seizure detection methods based on frequency domain processing. Rana et al. [36] proposed a technique based on multi-channel Electro-Cortico-Gram (ECoG) and the phase-slope index. Another technique was introduced depending on frequency-moment signatures to detect patient-specific seizures with a sensitivity of 91% [37]. Furthermore, several methods have been proposed based on dividing the EEG signals into time intervals, and then applying a suitable transform. Gabor transform, Fourier transform, and many other transforms have been used to obtain suitable seizure features. Zhou et al. [38] proposed another technique using lacunarity and Bayesian linear discriminant analysis for seizure detection with a sensitivity of 96.25%. Liu et al. [39] proposed a wavelet-transform-based technique, using SVM in long-term iEEG with a sensitivity of 94.46%, and a specificity of 95.26%.

The CNN-based classification methods achieve remarkable results on various datasets. To study these methods, several aspects should be taken into consideration, including the number and the architecture of CNNs, the dataset used for training, the type of loss function and the incorporated learning strategies. Vidyaratne et al. [40] proposed cellular neural networks and bi-directional recurrent neural networks to extract temporal features for seizure analysis. Shoeb et al. [41] presented a patient-specific ML technique based on the CHB-MIT dataset. They extracted spectral and spatial features and then combined non-EEG features to form feature vectors. Their approach detected 96% of 173 test seizures in an event-based assessment. Pramod et al. [42] and Turner et al. [43] used deep belief networks applied to multi-channel EEG data for seizure detection. Moreover, Kashif et al. [44] designed a hybrid Local Binary Pattern (LBP) wavelet-based approach to classify EEG signals for epilepsy patients. LBP is used to transform the EEG signal into a new signal, and then the Discrete Wavelet Transform (DWT) is employed to decompose the obtained signal. Linear Discriminant Analysis (LDA) classifier has been used for the classification process. Experiments were carried out on 105 seizures for 14 randomly-selected subjects of the CHB-MIT dataset.

Lorena et al. [45] developed a patient non-specific strategy for seizure detection based on the Stationary Wavelet Transform of EEG signals. Their approach was tested on scalp EEG records of 24-48 h for 18 epilepsy patients. Safi et al. [46] proposed a framework based on Convolutional Denoising Auto-encoder (CDA) for multivariate time series imputation. In addition, they performed a pre-processing step to encode time series data into 2D images using Gramian Angular Summation Field (GASF). Wang et al. [47] designed an approach to convert time series data into novel representations using Gramian Angular Field (GAF) and Markov Transition Field (MTF) images. Barra et al. [48] presented a method for forecasting certain patterns by applying DL technologies and encoding time series on GAF images. In [49], epileptic seizures have been classified based on the reinforcement learning technique. In this technique, Hilbert-Huang transform is used to extract 19 time-frequency domain features. Its classification accuracy reached 96.79%. In [50], seizure classification has been performed depending on brain activities. In addition, wavelet transform is used for EEG signal decomposition. Classification accuracy reached 89.60% using cubic SVM classifier and 87.00% using weighted KNN classifier.

3 Materials and methods

3.1 CHB-MIT dataset

The experiments have been carried out on large datasets to ensure generality. The CHB-MIT dataset [51] is a publicly-available dataset from physionet.org that contains 686 sEEG taken for 24 patients treated at Boston Children's hospital. Only 198 of the 686 records contain seizures. The worldwide 10-20 standard EEG electrode placement and labeling have been employed for dataset acquisition. However, 17 of the seizure files exhibited distinct channel montages. As a result, these 17 records have been eliminated from this study, leaving 181 seizure files. Table 1 provides detailed information about the dataset used to evaluate the proposed approach.

Table 1 Summary of the utilized EEG dataset

Patient No.	No. of Hours	No. of Seizures	Gender	Age
1	40.55	7	F	11
2	35.16	3	M	11
3	36	7	F	14
4	150.7	4	M	22
5	39	5	F	7
6	68.24	10	F	1.5
7	67.05	3	F	14.5
8	20	5	M	3.5
9	65.02	4	F	10
10	50.02	7	M	3
11	34.62	3	F	12
12	23.671	40	F	2
13	32	12	F	3
14	25.851	8	F	9
15	39.42	20	M	16
16	19	10	F	7
17	22	3	F	12
18	35.633	6	F	18
19	29.93	3	F	19
20	27.595	8	F	6
21	31.816	4	F	13
22	32	3	F	9
23	25.733	7	F	6
24	12	16	M	12.5

3.2 ML-based approach

Figure 1 depicts the main architecture of the proposed approach for seizure detection and prediction. EEG signal analysis involves segmentation, EMD, HHT, and ML classifier to detect epileptic seizures. The first step is the segmentation process, which involves dividing the EEG recording into small segments of a specific length. A window refers to the specific time frame or duration used to divide the EEG recording into smaller segments. The window size can have a significant impact on the analysis and interpretation of the EEG signals. A smaller window size will provide a higher temporal resolution and will allow for the detection of short-lived events, such as seizures. However, smaller window sizes can also increase the amount of noise, making it more difficult to detect seizures. On the other hand, larger window sizes will provide a lower temporal resolution but will reduce the amount of noise, making it easier to detect seizures. The segmentation process is followed by the application of the HHT on the segments. The HHT is a signal processing technique that can be used to decompose a non-linear and non-stationary signal into its IMFs. The HHT is based on the EMD and the Hilbert transform. The EMD decomposes the signal into a set of IMFs, each representing a different intrinsic oscillatory mode present in the signal [52–54]. The Hilbert transform is then applied on each IMF to obtain the corresponding instantaneous frequency. By applying the HHT on the segments, the proposed approach provides a detailed analysis of the EEG signal and extracts relevant features that can be used to detect seizures. The HHT allows for a frequency-time analysis of the EEG segments, providing further information about the signal dynamics, and the IMFs obtained from the EMD allow isolation of different intrinsic oscillatory modes present in the signal. After that, spectral entropies, sub-band energies, and higher-order statistics are used as features to classify the EEG segments as S or NS. These features are extracted from the segments after applying the HHT and are used to train ML models. Spectral entropies, such as Shannon, Tsallis, and Renyi entropies, are calculated from the power spectra of the signals. They can be used to distinguish S segments from NS segments. This can be done by comparing the entropy of the signal during S and NS states and identifying any significant differences in complexity. Sub-band energies represent the energy present in different frequency bands of the signal. They can provide information on the distribution of energy in different frequency bands. This strategy can be used to detect any changes in energy distribution that may be indicative of seizures. Higher-order statistics are statistical features that capture the characteristics of a signal beyond the traditional second-order features such as power and energy. Examples of higher-order statistics include kurtosis and skewness. These features can provide additional information about the signal that can be used to detect seizures. They can be used to detect any changes in the distribution of the signal that may be indicative of seizures. Overall, these features are chosen to reflect the characteristics of the EEG signal that can help to distinguish S from NS or PS segments. These features are then combined to provide a comprehensive analysis of the EEG signal. The features are fed into ML models like SVM, to classify the segments as S, NS, and PS. ML models are used to classify the EEG segments as S or NS based on the features extracted from the segments. The proposed approach depends on the use of three different types of ML models: SVM, KNN, and LR models. SVM is a supervised learning algorithm that creates a hyperplane or a set of hyperplanes in high-dimensional space to separate different classes. SVM is known for its ability to handle high-dimensional and non-linearly separable data, which makes it a good candidate for EEG signal analysis. KNN is a non-parametric tool that assigns a class label to a new data point based on the major class among its k-nearest neighbors. KNN is a simple and easy-to-implement algorithm that is known for its good performance on small datasets. LR is a supervised learning algorithm that models the relationship between a dependent variable and one or more independent variables by fitting a probability distribution function. LR is a simple and easy-to-implement algorithm that can be used to model the probability of an event occurring. These three algorithms have been selected as they are known to be good classifiers, and they have been widely used in EEG signal analysis. The tuning parameters of these models are presented in Table 2. The performance of the models has been evaluated using metrics such as accuracy, sensitivity, and specificity, and fine-tuned, accordingly. The combination of these ML models with the proposed feature extraction method, which gives spectral entropies, sub-band energies, and higher-order statistics, will provide a comprehensive analysis of the EEG signal and increase the chances of detecting seizures with high accuracy.

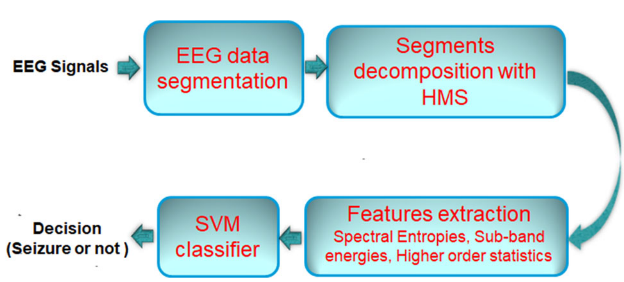

Fig. 1 Block diagram of the proposed epileptic seizure detection approach using HMS with different classifiers

Table 2 Tuning parameters definitions and their values for SVM, KNN, and LR classifiers in the proposed approach for seizure detection and prediction

Model	Parameters	Definition	Value or Function
SVM	Kernel function	Kernel function to transform the input data into a higher dimensional space, where it becomes linearly separable	Radial Basis Function (RBF)
	Regularization parameter (C)	A parameter that controls the trade-off between maximizing the margin and minimizing the mis-classification error	0.1
	Gamma	A parameter that controls the width of the RBF kernel	0.1
	Tolerance	A parameter that is used to stop the optimization process. Smaller tolerance values will result in more accurate solutions, but will also require more time to train the model.	10^{-4}
KNN	K	A parameter that represents the number of nearest neighbors used to classify a new data point.	5
	Distance metric	A parameter that represents the method used to measure the distance between data points.	Manhattan distance
	Weighting scheme	A scheme that represents the method used to assign a weight to each nearest neighbor, when classifying a new data point.	Distance-based weighting
	Normalization	A process that represents the method used to normalize the feature values.	Z-Score normalization
LR	Regularization parameter (C)	A parameter that controls the trade-off between maximizing the likelihood of the model and minimizing the complexity of the model.	0.1
	Optimization Algorithm	A tool that represents the method used to optimize the cost function.	Gradient Descent
	Tolerance	A parameter that is used to stop the optimization process. Smaller tolerance values will result in more accurate solutions, but will also require more time to train the model.	10^{-5}
	Penalty	A parameter that is used to specify the type of regularization.	LII

3.2.1 The Hilbert-Huang Transform (HHT) and its spectrum

The Hilbert transform is applied on each IMF component once the IMFs have been computed using the EMD [51].

$$H[q_i(t)] = \frac{1}{\pi}\int_{-\infty}^{+\infty}\frac{q_i(\tau)}{t-\tau}d\tau \tag{1}$$

where $q_i(\tau)$ and $H[q_i(t)]$ form a complex conjugate pair that specifies an analytic signal $Z_i(t)$.

$$Z_i(t) = q_i(t) + jH[q_i(t)] \tag{2}$$

It can be represented as:

$$Z_i(t) = a_i(t)exp(j\omega_i(t)) \tag{3}$$

where $a_i(t)$ is the amplitude and $\theta_i(t)$ represents the phase.

$$a_i(t) = \sqrt{c_i(t) + H^2[c_i(t)]} \tag{4}$$

$$\theta_i(t) = arctan\left(\frac{H[c_i(t)]}{c_i(t)}\right) \tag{5}$$

Thus, the instantaneous frequency $\omega_i(t)$ can be defined as:

$$\omega_i(t) = \frac{d\theta_i(t)}{dt} \tag{6}$$

Therefore, the original data can be defined as follows:

$$E(t) = Re\sum_{i=1}^{L}a_i(t)exp(j\int\omega_i(t)dt) \tag{7}$$

where the residue $u_l(t)$ has been discarded. Hilbert-Huang spectrum represents the instantaneous amplitude and the instantaneous frequency in a three-dimensional plot, where the amplitude represents the height in the time-frequency plane.

$$H(\omega, t) = Re\sum_{i=1}^{L}a_i(t)exp(j\int\omega_i(t)dt) \tag{8}$$

Finally, the marginal spectrum $h(\omega)$ can be expressed as follows:

$$h(\omega) = \int_0^T H(\omega, t)dt \tag{9}$$

The marginal spectrum gives a measure of the total energy contribution from each frequency value. Thus, the local marginal spectrum of each IMF component is defined as:

$$h_i(\omega) = \int_0^T H_i(\omega, t)dt \tag{10}$$

The local marginal spectrum $h_i(\omega)$ gives a representation of the total amplitude contribution versus frequency ω that we are interested in.

3.2.2 Feature extraction

The distinctive attributes of a signal are represented by features. The next step is to identify discriminating features of EEG signals for different classes. Different attributes, namely, Renyi entropy, Tsallis entropy, Shannon entropy, sub-band energies, skewness, and kurtosis are extracted and used as the main features.

1. **Spectral Entropies** Entropy is an indication of disorder in physical systems. It is related to the amount of information obtained by observations of disordered systems. Spectral entropy depends on the PDF of spectral probabilities. Flat probability distribution means high entropy. On the other hand, peaked probability distribution means low entropy [56]. The Fourier-spectrum-based entropies have a great contribution to the success of EEG seizure detection problems [56, 57]. Entropy is a statistical measure of the variability within the EEG signal. HMS-based entropy is exploited to provide a better performance in EEG signal analysis, due to its highest performance in non-stationary signal analysis. Three different statistical entropies are employed and discussed. To estimate the entropy, the spectrum should be normalized to obtain the probability mass function.

$$p_i = \frac{P_i}{\sum_{i=1}^n P_i} \tag{11}$$

where P_i represents the energy content corresponding to the frequency component i. Moreover, p_i represents the probability density function of the spectrum. Then, the Shannon entropy is expressed as follows [58]:

$$SEN = -\sum_{i=1}^n p_i log p_i \tag{12}$$

where p_i is the probability density of the spectrum:

$$\sum_{i=1}^n p_i = 1 \tag{13}$$

The Renyi entropy is expressed as follows [59]:

$$REN_\alpha = \frac{1}{1-\alpha} log \sum_{i=1}^n p_i^\alpha \tag{14}$$

The Tsallis entropy is expressed as follows [60]:

$$TEN_\alpha = \frac{1}{1-\alpha}(1 - \sum_{i=1}^n p_i^\alpha) \tag{15}$$

where α is a tuning factor to generate a profile that is less sensitive to the shape of probability distributions. In this paper, α is set to 2 for both Renyi and Tsallis entropies.

2. **Sub-band energies** Sub-bands are obtained with digital filters to extract features from each one. The used sub-bands are delta: 0-4 Hz, theta: 4-8 Hz, alpha: 8-12 Hz, beta: 12-30 H, and gamma: 30-50 Hz [61]. The energy distribution between S and NS segments is quite different [62]. For a normal EEG segment, the energy is included in the delta wave, while the same wave in the seizure contains a small proportion of the total energy. Therefore, sub-band energy is effective in EEG seizure detection. The sub-band energies in HMS are expressed as follows [63]:

$$e_i = \sum_{f=0}^{k-1} h_i^2 \tag{16}$$

where k represents the total number of frequency bins and h_i is the i^{th} sub-band of the spectrum.

3. **Higher-order statistics** The distribution of the samples of an EEG signal is characterized by its level of dispersion and asymmetry μ. Hence, skewness and kurtosis are utilized as main features for the EEG seizure detection problem. For an N-point sequence, $X = x_1, x_2, ..., x_N$, the corresponding skewness β_1, and kurtosis β_2 are calculated as follows [64]:

$$\beta_1 = \frac{1}{N}\sum_{i=1}^N (\frac{x_i - \mu}{\sigma})^3 \tag{17}$$

$$\beta_2 = \frac{1}{N}\sum_{i=1}^N (\frac{x_i - \mu}{\sigma})^4 \tag{18}$$

where μ represents the sample mean of the sequence and σ denotes its Standard Deviation (SD). The skewness and kurtosis are computed from the second-order, third-order, and fourth-order moments.

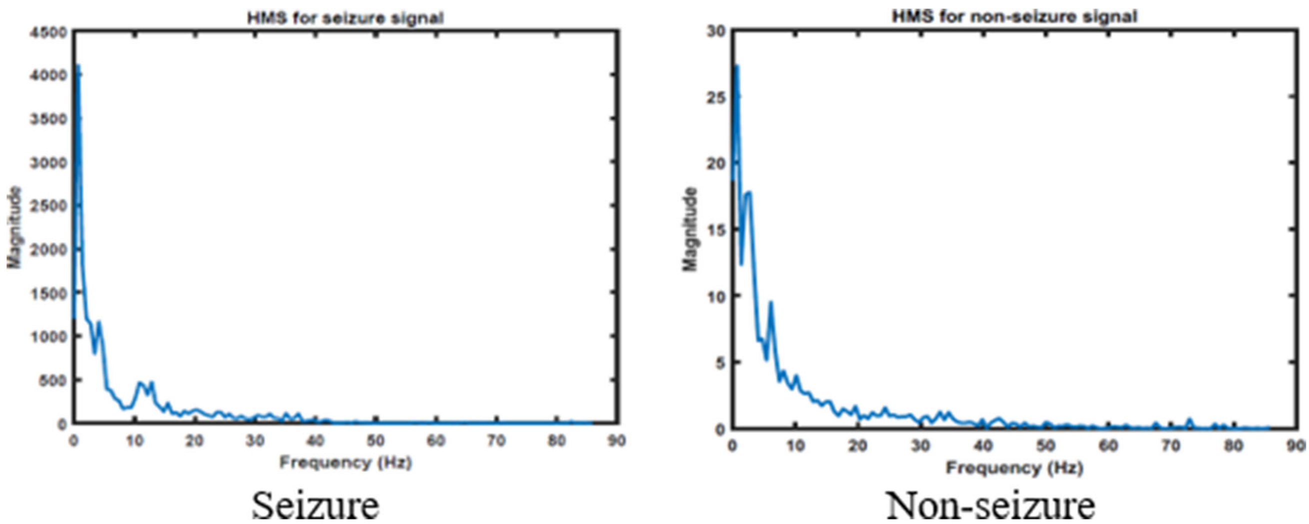

Fig. 2 Comparison of HHT spectral analysis of Seizure (S) and Non-Seizure (NS) EEG signals for the frequency band of 0-90 Hz

3.2.3 Performance metrics

The proposed approach performance is evaluated using standard metrics such as sensitivity, specificity, and accuracy [65, 66]. T_P is the total number of true seizure events, whereas T_n denotes the total number of true normal events. The variables F_P (False positive) and F_n (False negative) denote the total number of erroneous seizures and normal events, respectively.

$$Sensitivity = \frac{T_p}{T_p + F_n} \times 100\% \tag{19}$$

$$Specificity = \frac{T_n}{T_n + F_p} \times 100\% \tag{20}$$

$$Accuracy = \frac{T_p + T_n}{T_p + T_n + F_p + F_n} \times 100\% \tag{21}$$

3.2.4 Results and discussion

The proposed approach performance is evaluated on the CHB-MIT dataset [51]. EMD processing is performed, and hence, HHT is applied on the EEG signals. Then, the HMS can be calculated. Figure 2 shows the HMS spectrum for S and NS EEG signals. It is clear that the magnitude of the HMS is different for S and NS activities.

Figure 3 illustrates the spectral entropies distribution for S and NS activities for multi-channel EEG signals. The mean and SD for the features collected for the different activities of EEG signals are shown in Tables 3 and 4. The mean values for S, NS, and PS activities are all distinct. Except for the kurtosis, all features have a small SD. Furthermore, in comparison with other activities, the mean values of kurtosis for S, NS, and PS activities are relatively large. The kurtosis is progressively decreased as the IMF level increases (Table 5).

Table 6 presents the obtained results for SVM, KNN, and LR classifiers. An accuracy of 100%, a sensitivity of 100%, and a specificity of 100% are obtained for both SVM, KNN, and LR classifiers. For the last case, which is especially important during on-line detection of seizure occurrence for an epilepsy patient, an accuracy of 100%, a sensitivity of 100% and a specificity of 100% are obtained for both SVM, KNN, and LR classifiers. Thus, these results might be valuable for implantable devices such as the cranial implanted Respirator Neuro-Simulator (RNS) [67]. The proposed approach holds prospect for such devices, since it can detect seizures accurately as evidenced from the ability to discriminate pre-seizure from seizure classes with a 100% accuracy (Fig. 4).

3.3 CNN-based approach

This proposed approach for seizure detection and prediction is described in Fig. 5. It adopts the spectrogram estimation process to transform the EEG signals into an image-like format. The spectrogram of an EEG signal is an estimation of the time evolution of the EEG frequency content. After image acquisition, a CNN is used to extract deep features from the spectrogram images. The CNN is responsible for taking an input image and assigning learnable weights and biases to different objects in that image. Convolutional, pooling, and depth concatenation layers are used for the process of feature extraction. Finally, the extracted deep features are used for classification to obtain the detection and prediction results.

3.3.1 Spectrogram estimation

A spectrogram shows how the frequency content of a signal changes with time. The spectrogram graph shows the

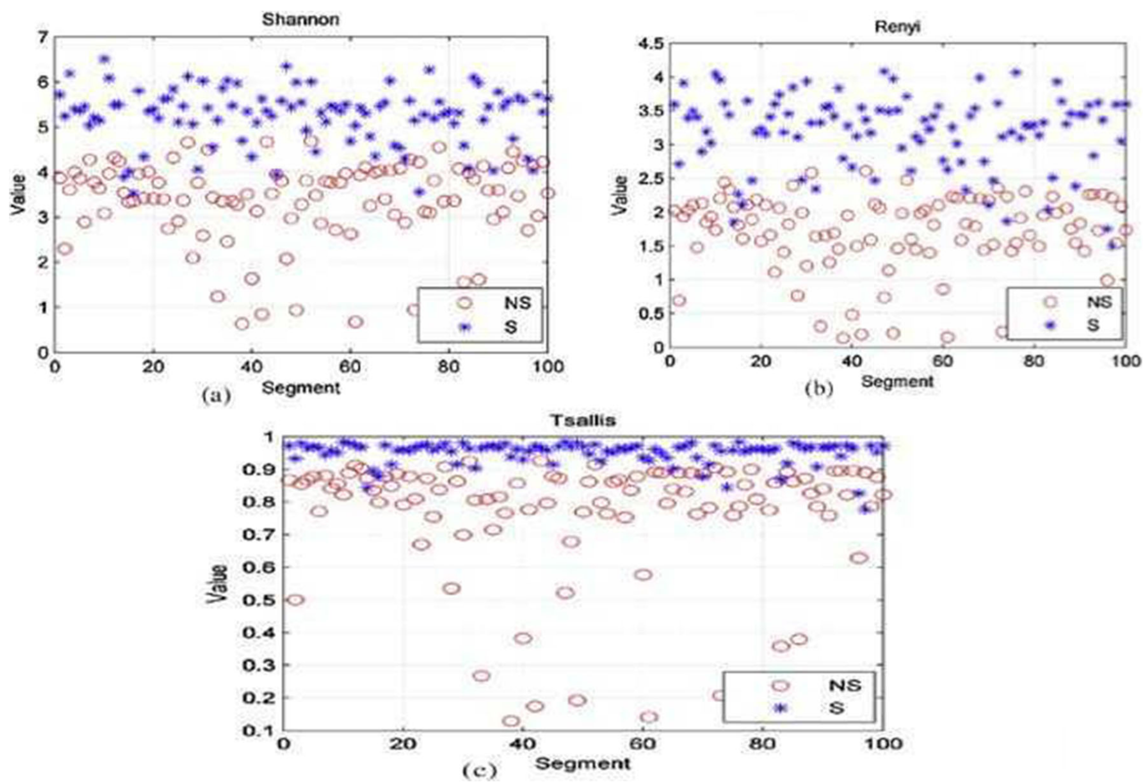

Fig. 3 Entropy distribution of Shannon (a), Renyi (b), and Tsallis (c) of Seizure (S) and Non-Seizure (NS) EEG signals for CHB-MIT dataset

Table 3 Mean values of entropies of S, NS and PS activities (SD shown in parenthesis) for the CHB-MIT dataset

	NS			PS			S		
	Shannon	Renyi	Tsallis	Shannon	Renyi	Tsallis	Shannon	Renyi	Tsallis
IMF1	4.3706	3.8382	0.9744	3.7977	3.0006	0.9223	3.8515	3.2291	0.8895
	(0.4519)	(0.5674)	(0.0174)	(0.8838)	(0.9236)	(0.0835)	(1.4323)	(1.5181)	(0.1456)
IMF2	4.7507	4.3060	0.9840	4.5312	3.9908	0.9790	4.8051	4.4925	0.9875
	(0.3521)	(0.5204)	(0.0131)	(0.3659)	(0.4912)	(0.0122)	(0.3791)	(0.4442)	(0.0065)
IMF3	4.5356	4.0332	0.9795	4.3750	3.7635	0.9738	4.5242	4.0834	0.9818
	(0.3503)	(0.4831)	(0.0154)	(0.3537)	(0.4806)	(0.0142)	(0.2631)	(0.3595)	(0.0091)
IMF4	4.3239	3.7328	0.9735	4.1856	3.52461	0.9672	4.2474	3.6896	0.9729
	(0.3251)	(0.4127)	(0.0147)	(0.3617)	(0.4383)	(0.0176)	(0.2711)	(0.3725)	(0.0129)
IMF5	4.0547	3.3446	0.9621	3.9014	3.1683	0.9528	3.9760	3.2830	0.9589
	(0.3038)	(0.3562)	(0.0169)	(0.3552)	(0.4271)	(0.0322)	(0.3363)	(0.3877)	(0.0231)
IMF6	3.7622	2.9144	0.9437	3.6417	2.8494	0.9369	3.6202	2.8083	0.9340
	(0.2544)	(0.2651)	(0.0176)	(0.3311)	(0.3655)	(0.0371)	(0.3547)	(0.3882)	(0.0354)
IMF7	3.3683	2.4255	0.9054	3.3117	2.4309	0.9068	3.3995	2.4397	0.9073
	(0.3281)	(0.3393)	(0.0430)	(0.2994)	(0.3232)	(0.0359)	(0.2975)	(0.3269)	(0.0382)
IMF8	2.8289	1.6579	0.8030	2.6209	1.5346	0.7748	2.6766	1.5177	0.7719
	(0.2474)	(0.2619)	(0.0518)	(0.3123)	(0.2920)	(0.0709)	(0.2975)	(0.2769)	(0.0698)
IMF9	2.1142	1.0196	0.6321	2.0599	1.0061	0.6267	2.0648	0.9713	0.6153
	(0.2204)	(0.2060)	(0.0689)	(0.2735)	(0.2065)	(0.0753)	(0.2265)	(0.1827)	(0.0673)
IMF10	1.6243	0.6819	0.4906	1.5542	0.6508	0.4740	1.5944	0.6541	0.4764
	(0.1817)	(0.1237)	(0.0612)	(0.2044)	(0.1300)	(0.0671)	(0.1867)	(0.1218)	(0.0610)

Table 4 Mean values of skewness and kurtosis of S, NS and PS activities (SD shown in parenthesis) for CHB-MIT dataset

	Non-Seizure		Pre-Seizure		Seizure	
	Skewness	Kurtosis	Skewness	Kurtosis	Skewness	Kurtosis
IMF1	0.5657 (0.7585)	3.5376 (2.0221)	3.7993 (4.3115)	43.5668 (58.3711)	4.5030 (5.0127)	55.2191 (71.7170)
IMF2	1.2270 (0.1051)	3.4819 (0.3977)	1.3135 (0.2739)	3.9643 (1.6347)	1.3809 (0.3107)	4.0160 (1.5803)
IMF3	2.1869 (0.1069)	7.4109 (0.7320)	2.2035 (0.2496)	7.7050 (2.2554)	2.2155 (0.3909)	7.7862 (4.6256)
IMF4	3.2745 (0.1354)	14.6212 (1.1885)	3.3475 (0.3020)	15.4304 (3.7378)	3.3044 (0.5531)	15.6607 (7.5842)
IMF5	4.8023 (0.2333)	29.9230 (3.0580)	4.8657 (0.4248)	30.8909 (6.9060)	4.7642 (0.5686)	30.3498 (9.4347)
IMF6	6.9888 (0.3599)	62.9239 (6.9274)	6.9959 (0.3963)	62.8244 (7.6077)	6.9265 (0.6010)	62.4425 (11.7561)
IMF7	8.2815 (0.3144)	81.6593 (6.7364)	8.2954 (0.3556)	81.7209 (7.3254)	8.6577 (0.5184)	89.6726 (11.3421)
IMF8	11.6449 (0.3382)	156.2259 (8.1622)	11.5788 (0.2988)	154.3954 (7.3454)	11.9603 (0.4945)	163.6994 (11.9010)
IMF9	13.4746 (0.1945)	198.7594 (4.7042)	13.4497 (0.2110)	198.1396 (5.1438)	13.5202 (0.4329)	199.7580 (10.5091)
IMF10	14.3710 (0.1359)	219.5694 (3.2596)	14.3747 (0.1495)	219.6605 (3.6079)	14.4454 (0.2056)	221.2934 (4.9348)

energy content of a signal expressed as a function of time and frequency. The produced graph shows amplitude-dependent colors with the horizontal and vertical axes as time and frequency. The first step to calculate the spectrogram is the segmentation of the EEG signal to equal-length windows. The window size should depend on the non-stationary nature of the EEG signal. The idea here is that the spectral properties of an EEG non-stationary signal can be displayed through a series of spectral snapshots. As a non-stationary signal, EEG signal frequencies change with time. Choosing the segment length is the most important step in the spectrogram estimation, because it determines and fixes the frequency resolution. The segment length (time resolution) must be short enough. In this proposal, we use a sliding window of size 1 second, and a temporal resolution of 1 second with no overlapping. The next step in the signal analysis is the computation of the spectrum to get the short-time Fourier transform. Finally, the power of each spectrum is displayed segment by segment. These spectra are laid side by side to form the image. A magnitude-dependent color map is produced as an image. Figure 6 shows a number of spectrogram images including the NS, PS, and S cases. These images belong to patients 1, 2, and 3.

3.3.2 Convolutional neural network (CNN)

The CNN architecture is inspired by the organization of the visual cortex. In addition, this architecture is similar to the connectivity pattern of neurons in the human brain. Individual neurons respond to stimuli only in a restricted region of the visual field known as the receptive field. Such fields overlap to cover the entire visual area. The CNN depends on relevant filters to extract the temporal and spatial dependencies in an image. In this work, we propose a CNN model in which the residual learning and depth concatenation strategies have been adopted as illustrated in Fig. 7. The size of the input layer is $227 \times 227 \times 3$. The proposed model contains thirteen convolutional layers, each of which produces an output feature map $f_{x,y,k}^{c,l}$ for a particular layer l and an input $f_{x,y}^{O_p,l-1}$ [18]:

$$f_{x,y,k}^{c,l} = {W_k^l}^T f_{x,y}^{O_p,l-1} + b_k^l \tag{22}$$

where W_k^l are the shared weights, b_k^l is the bias and c denotes convolution. O_p represents the input image, for $l = 1$, while it represents convolution, pooling or activation, for $l > 1$.

Table 5 Mean values of sub-band energies of S, NS and PS activities (SD shown in parenthesis) for CHB-MIT dataset

	Non-Seizure					Pre-Seizure					Seizure				
	e1	e2	e3	e4	e5	e1	e2	e3	e4	e5	e1	e2	e3	e4	e5
IMF1	31.9264	33.2604	34.1938	36.6188	36.2542	36.1904	33.4197	33.9807	36.7524	36.8101	41.1848	37.9970	38.7268	41.1628	40.5660
	(1.5420)	(1.3732)	(1.3342)	(0.9322)	(0.5510)	(2.7783)	(1.5407)	(1.1376)	(0.9147)	(0.5244)	(3.2314)	(1.2039)	(0.9058)	(0.7692)	(0.5998)
IMF2	33.4410	35.0816	36.4441	38.5725	37.4205	34.3234	35.6716	37.0752	39.1960	38.0375	38.4263	40.0677	41.3077	43.3533	42.0549
	(0.7542)	(0.7485)	(0.7027)	(0.5751)	(0.5988)	(0.7483)	(0.7417)	(0.7305)	(0.5822)	(0.5664)	(1.0326)	(1.2074)	(1.1389)	(0.9607)	(0.7376)
IMF3	36.5582	38.9271	39.0486	39.0329	37.0131	37.2082	39.4577	39.5371	39.5670	37.8255	41.3288	43.4967	43.4979	43.5906	41.4915
	(0.6779)	(0.6151)	(0.6075)	(0.5966)	(2.9492)	(0.6636)	(0.6502)	(0.5964)	(0.5838)	(0.5983)	(0.8485)	(0.8172)	(0.8215)	(0.8474)	(0.8694)
IMF4	39.9166	39.8709	38.8111	38.6775	36.9262	40.4502	40.4559	39.3605	39.2321	37.5275	44.3444	44.2365	43.1966	43.1737	41.0463
	(0.6390)	(0.6168)	(0.6138)	(0.5918)	(0.5683)	(0.6007)	(0.6141)	(0.6188)	(0.5888)	(0.5863)	(0.8483)	(0.8638)	(0.8502)	(0.8786)	(0.9260)
IMF5	41.0588	39.5823	38.4544	38.3157	36.5285	41.6472	40.1490	39.0016	38.8898	37.1627	45.3524	43.8914	42.8500	42.7518	40.7563
	(0.6068)	(0.6141)	(0.6031)	(0.6033)	(0.6135)	0.5986	(0.5891)	(0.6158)	(0.6024)	(0.5781)	(0.8768)	(0.8452)	(0.9092)	(0.8975)	(0.8989)
IMF6	41.7129	39.2219	38.1195	37.9831	36.1715	42.3032	39.8183	38.6249	38.5532	36.8177	46.0260	43.5557	42.5241	42.3860	40.3168
	(0.6043)	(0.6148)	(0.5983)	(0.6049)	(0.6208)	(0.5906)	(0.5980)	(0.5837)	(0.6042)	(0.5983)	(0.9228)	(0.8911)	(0.9838)	(0.8869)	(0.8805)
IMF7	42.1832	38.9462	37.8222	37.6693	35.8838	42.7839	39.5112	38.3789	38.2159	36.5301	46.5225	43.2339	42.1847	42.0728	40.1586
	(0.6102)	(0.6308)	(0.6051)	(0.5899)	(0.5861)	(0.5800)	(0.5991)	(0.6223)	(0.6028)	(0.6319)	(0.8978)	(0.8790)	(0.8981)	(0.9033)	(1.0139)
IMF8	42.7310	38.6760	37.5512	37.4127	35.6390	43.3294	39.2677	38.1402	37.9403	36.2065	47.0806	43.0139	41.9086	41.8742	39.7770
	(0.6134)	(0.6291)	(0.6083)	(0.5846)	(0.6019)	(0.5818)	(0.6155)	(0.6445)	(0.5805)	(0.5895)	(0.8908)	(0.9294)	(0.9058)	(1.0102)	(0.9696)
IMF9	43.1506	38.4322	37.2987	37.1692	35.3738	43.7408	39.0434	37.9149	37.6942	35.9860	47.4548	42.7404	41.6402	41.6113	39.6892
	(0.6078)	(0.6264)	(0.6113)	(0.5874	(0.6115)	(0.5859)	(0.6205)	(0.6003)	(0.5757)	(0.6082)	(0.8845)	(0.9011)	(0.9470)	(0.9544)	(0.9836)
IMF10	43.4411	38.2179	37.1051	36.9503	35.1560	44.0334	38.8396	37.6977	37.5003	35.7765	47.7457	42.6179	41.4622	41.4151	39.4772
	(0.6010)	(0.6216)	(0.6041)	(0.5988)	(0.6028)	(0.5822)	(0.6086)	(0.6551)	(0.6040)	(0.6026)	(0.8907)	(0.9420)	(0.9738)	(0.9761)	(1.0614)

Table 6 Classification Performance using SVM, KNN, and LR classifiers for CHB-MIT dataset

Cases	SVM			KNN			LR		
	Accuracy	Sensitivity	Specificity	Accuracy	Sensitivity	Specificity	Accuracy	Sensitivity	Specificity
S, NS	100	100	100	100	100	100	100	100	100
NS, PS	100	100	100	100	100	100	100	100	100

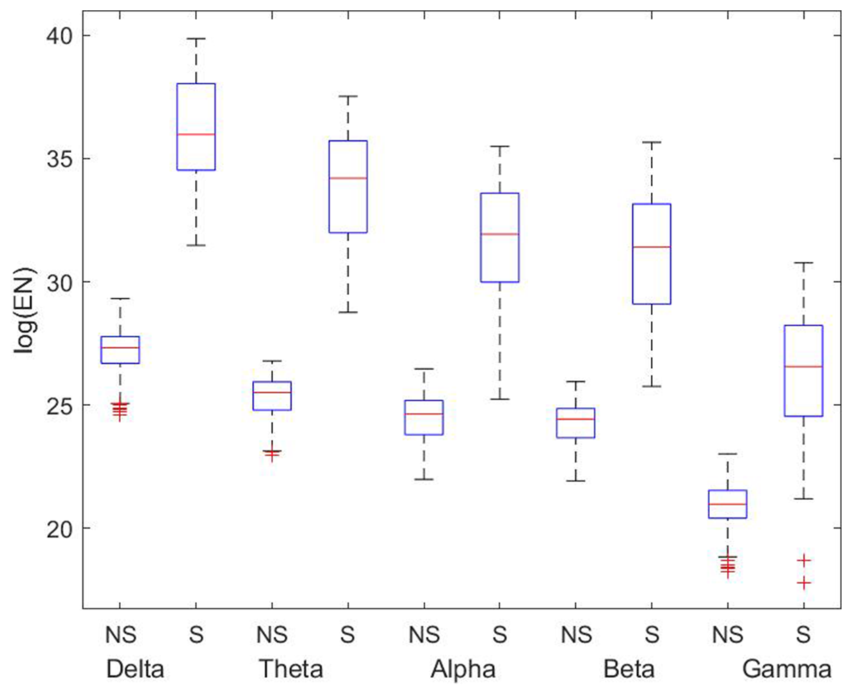

Fig. 4 Box plot of each sub-band energy features for S and NS activities

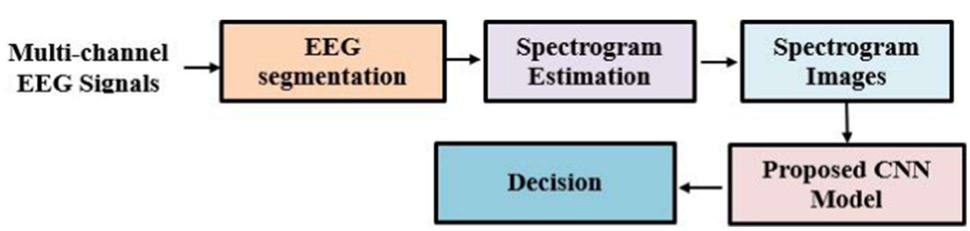

Fig. 5 Block diagram of the proposed CNN-based approach

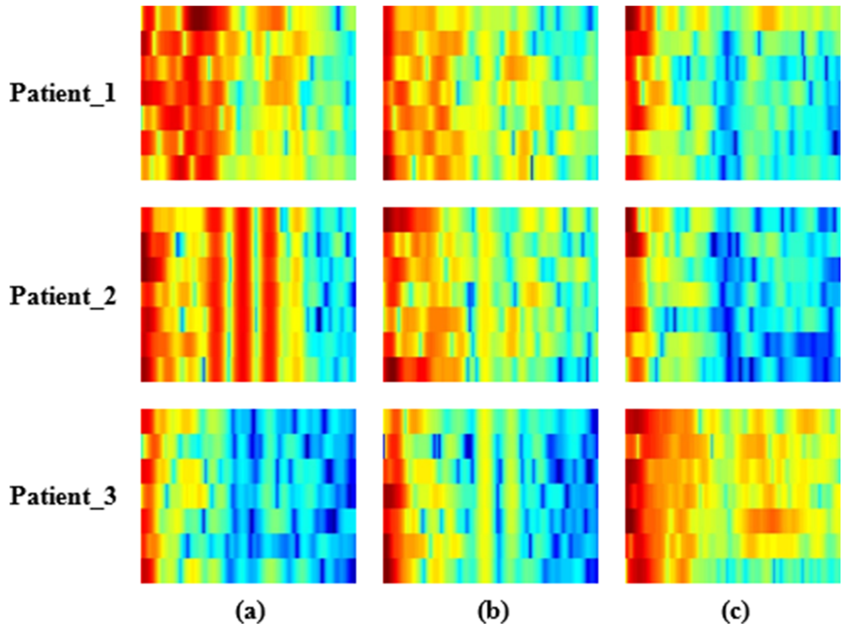

Fig. 6 Various spectrogram images for patients 1, 2, and 3: (a) NS case, (b) PS case, and (c) S case

Furthermore, we use different kernels for each convolutional layer. For example, layers (1, 6, 7, 12, and 13) have 192 kernels, layers (3, 5, 9, and 11) have 128 kernels, and layers (2, 4, 8, and 10) have 64 kernels. All layers have kernels of size 3×3 except layers 2 and 8 that have kernels of size 1×1. Each convolutional layer is followed by a Rectified Linear Unit "ReLU" activation function. This function transforms the weighted sum of inputs that goes into the artificial neurons.

In addition, a residual learning strategy is applied. This strategy is used to optimize the loss of CNNs in an easy way. The output of a residual block R can be expressed as:

$$f_{x,y,k}^{R,l} = f_{x,y}^{O_p,l-q} + F(f_{x,y}^{O_p,l-q}, W_k) \tag{23}$$

where $f_{x,y}^{O_p,l-q}$ is the input feature map, $F(.)$ is the residual mapping to be learned, and q is the total number of stacked layers. The proposed model includes four residual learning blocks. Each block includes a depth concatenation layer to increase the depth of the feature map by concatenating the feature maps that are generated by various filter sizes. The 1^{st} depth layer concatenates the output from the 3^{rd} and 5^{th} convolutional layers. The 2^{nd} depth layer concatenates the output from the 1^{st} and 6^{th} convolutional layers. The 3^{rd} depth layer concatenates the output from the 9^{th} and 11^{th} convolutional layers. Finally, the 4^{th} depth layer concatenates the output from the 7^{th} and 12^{th} convolutional layers. By adding the concatenation layers, the number of units at each stage can be increased without an uncontrolled blow-up in the computational complexity at later stages. The improvement of the computational resources allows for increasing the number of stages and the width of each stage of a CNN. Moreover, maximum pooling, fully-connected, and softmax layers are found in the proposed model. The maximum pooling layer computes the maximum value in a local spatial neighborhood, and then reduces spatial resolution. Fully-connected and softmax layers are used for classification and computing the loss, respectively. Table 7 provides the number of kernels and the size of each kernel for each convolutional layer.

3.3.3 Experimental results

Experiments are carried out on the signals of a group of patients from the CHB-MIT dataset. The used dataset is divided into three classes, namely NS, PS, and S. The performance of the proposed approach is measured in terms of accuracy, specificity, precision, sensitivity, and F-score. Moreover, the performance of the proposed approach is compared with those of pre-trained CNN models such as VGG19, ResNet101, and Inceptionv3.

Our target is to reach the optimal performance of the proposed CNNs. To achieve that, we have to select the Optimization Algorithm (OA) to be used and adjust the values of various hyperparameters such as weight decay, momentum value, mini-batch size, maximum epochs, and learning rate.

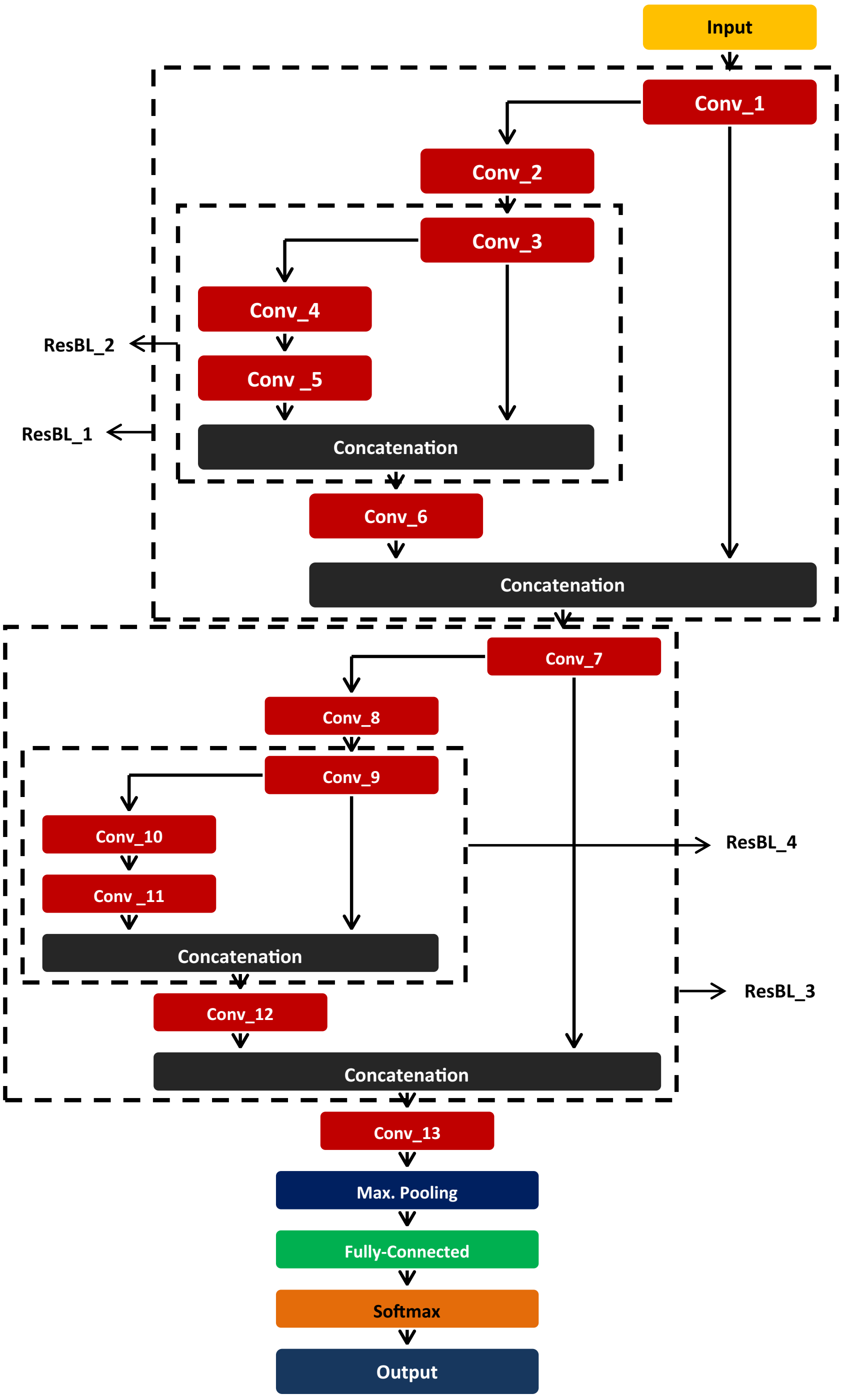

Fig. 7 The architecture of the proposed CNN model

- The OAs are mainly used to reduce the losses by changing weights and learning rate. Here, three optimization algorithms are selected, namely Adaptive Moment estimation (Adam), Root Mean Square propagation (RMSprop), and Stochastic Gradient Descent with Momentum (SGDM).
- Weight decay is a DL technique that adds a penalty term to the cost function to shrink the weights during back-propagation. The best value of weight decay is between 0 and 0.1. Here, the weight decay is set to 5×10^{-4}.
- Momentum is a gradient-descent algorithm used to overcome the oscillations of the cost across flat spots and noisy gradients of the search space. The momentum value is set to 0.9.
- Mini-batch size is defined as the amount of data included in each epoch weight change. Each epoch consists of one

Table 7 The number and size of kernels for each convolutional layer of the proposed CNN model

Convolutional Layer	Number of Kernels	Kernel Size
Conv_1	192	3 × 3
Conv_2	64	1 × 1
Conv_3	128	3 × 3
Conv_4	64	3 × 3
Conv_5	128	3 × 3
Conv_6	192	3 × 3
Conv_7	192	3 × 3
Conv_8	64	1 × 1
Conv_9	128	3 × 3
Conv_10	64	3 × 3
Conv_11	128	3 × 3
Conv_12	192	3 × 3
Conv_13	192	3 × 3

forward pass and one back-propagation pass over all the training samples. The mini-batch size is set to 32. Also, we select the maximum epochs to be 5.

– Learning rate is a parameter used to adjust the CNN model in response to the estimated error, when the weights are updated. We select three values of learning rate, namely 0.1, 0.01, and 0.001.

Table 8 shows the performance of the proposed CNN. We consider the data of patient 1 and the classification scenario of NS vs. PS. As mentioned before, we have three classes for each patient. All NS images of all patients are grouped together under the same class NS, and this is also applied to PS and S images. We have 10,000 images for each class. These images are divided into 70% for training and 30% for testing. We intend to perform three scenarios of classification. In the 1^{st} scenario, classification is performed between NS and PS classes. The 2^{nd} scenario provides the classification results between NS and S classes. Finally, the 3^{rd} scenario differentiates between NS, PS, and S classes, as shown in Table 9. Figures 8, 9 and 10 introduce the ROC and precision sensitivity curves for PS and S, S and NS and finally, PS, S, and NS cases, respectively.

The results demonstrate the effectiveness of using CNN models for EEG signal classification and seizure detection. The proposed CNN model achieved an accuracy of 97.66% for NS versus PS, 95.59% for NS versus S, and 94.51% for NS versus S versus PS cases. This accuracy is significantly higher than that of other models used in this study, such as VGG19, ResNet101, and Inceptionv3. The high accuracy of the proposed CNN model is attributed to its ability to extract features from the EEG signals that are more relevant to the task of seizure detection. The CNN model uses a combination of residual learning convolutional and pooling layers to extract features from the EEG signals, which allows it to learn complex patterns in the data. Additionally, the use of a large number of parameters in the CNN model allows it to capture more information from the EEG signals, which in turn leads to better performance. In terms of sensitivity, precision, and F-score, the proposed CNN model also outperforms the other models. The sensitivity, precision, and F-score of the proposed CNN model are 95.79%, 94.86%, and 95.32%, respectively, for NS versus PS, 94.73%, 93.68% and 94.2%, respectively, for NS versus S, and 93.04%, 92.47%, and 92.75%, respectively, for NS versus S versus PS cases. Hence, the proposed CNN model is not only accurate, but also highly specific and sensitive in identifying seizures.

However, it is important to note that the results presented here are based on a specific dataset, the CHB-MIT dataset, which contains 6 male and 18 female subjects. Therefore, it is essential to test the proposed CNN model on other datasets

Table 8 Performance of the proposed CNN for different optimization algorithms and learning rates

OA	Learning rater	Accuracy	Specificity	Sensitivity	Precision	F-score
	0.1	0.9573	0.9586	0.9432	0.9469	0.945
SGDM	0.01	0.9697	0.9713	0.9529	0.9618	0.9573
	0.001	0.9788	0.9798	0.9626	0.9721	0.9673
	0.1	0.9548	0.956	0.9457	0.9524	0.949
RMSprop	0.01	0.9558	0.9567	0.9437	0.9517	0.9476
	0.001	0.9536	0.9542	0.9429	0.9476	0.9452
	0.1	0.9655	0.9667	0.9445	0.9624	0.9533
Adam	0.01	0.9682	0.9695	0.9515	0.9637	0.9575
	0.001	0.9673	0.9685	0.9523	0.9632	0.9577

Table 9 Classification performance using CNN-based model with CHB-MIT dataset

Scenairo	Method	Accuracy	Sensetivity	Precision	Specificity	F-score
NS and PS	VGG19	88.7	88.16	86.96	88.89	87.55
	ResNet101	91.65	90.8	90.06	91.73	90.42
	Inceptionv3	94.4	93.87	92.67	94.57	93.26
	Proposed CNN	97.66	95.79	94.86	97.81	95.32
NS and S	VGG19	86.09	85.28	84.63	86.21	84.95
	ResNet101	89.18	88.45	87.8	89.34	88.12
	Inceptionv3	91.92	90.97	90.67	92.09	90.81
	Proposed CNN	95.59	94.73	93.68	95.72	94.2
NS, PS, and S	VGG19	83.66	82.86	82.16	83.78	82.5
	ResNet101	85.84	85.19	84.94	85.96	85.06
	Inceptionv3	89.15	88.37	87.81	89.27	88.08
	Proposed CNN	94.51	93.04	92.47	94.64	92.75

to confirm its generalizability. Additionally, the used dataset is not large enough for generalization.

3.4 Comparison with the state-of-the-art methods

A comparison between the proposed approaches and other published ones on the CHB-MIT dataset is presented in Table 10. It is clear that the proposed approaches achieve better results than those of the state-of-the-art methods. It produces improvement in terms of accuracy for the classification of NS and S classes. It provides an accuracy that reaches 100% and 95.59% with ML-based and CNN-based classification, respectively. In addition, it outperforms the other methods for the classification of PS and NS classes. It provides an accuracy that reaches 100% and 97.66% with ML-based and CNN-based classification, respectively.

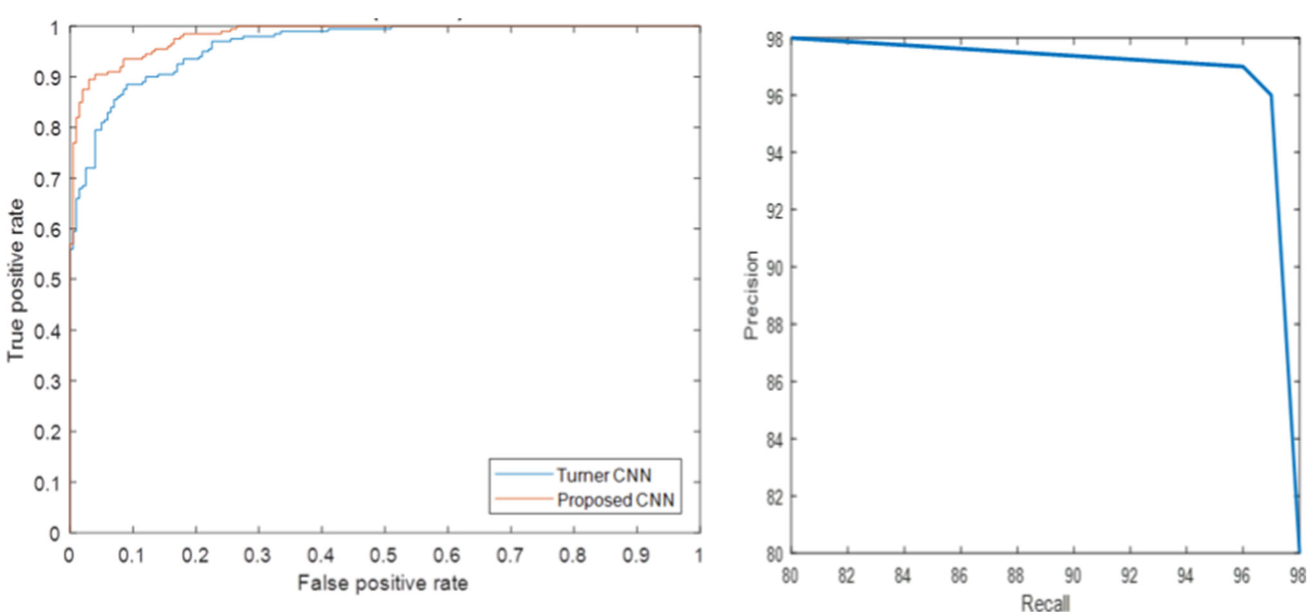

Fig. 8 ROC and precision recall curves for PS versus S cases

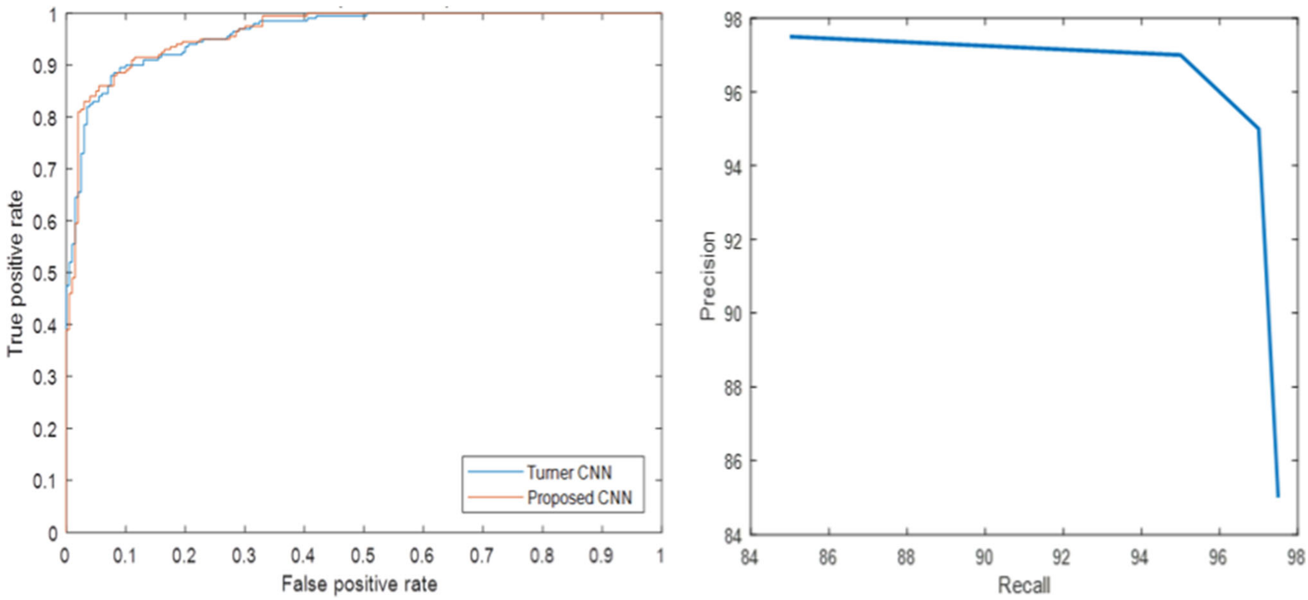

Fig. 9 ROC and precision recall curves for S versus NS cases

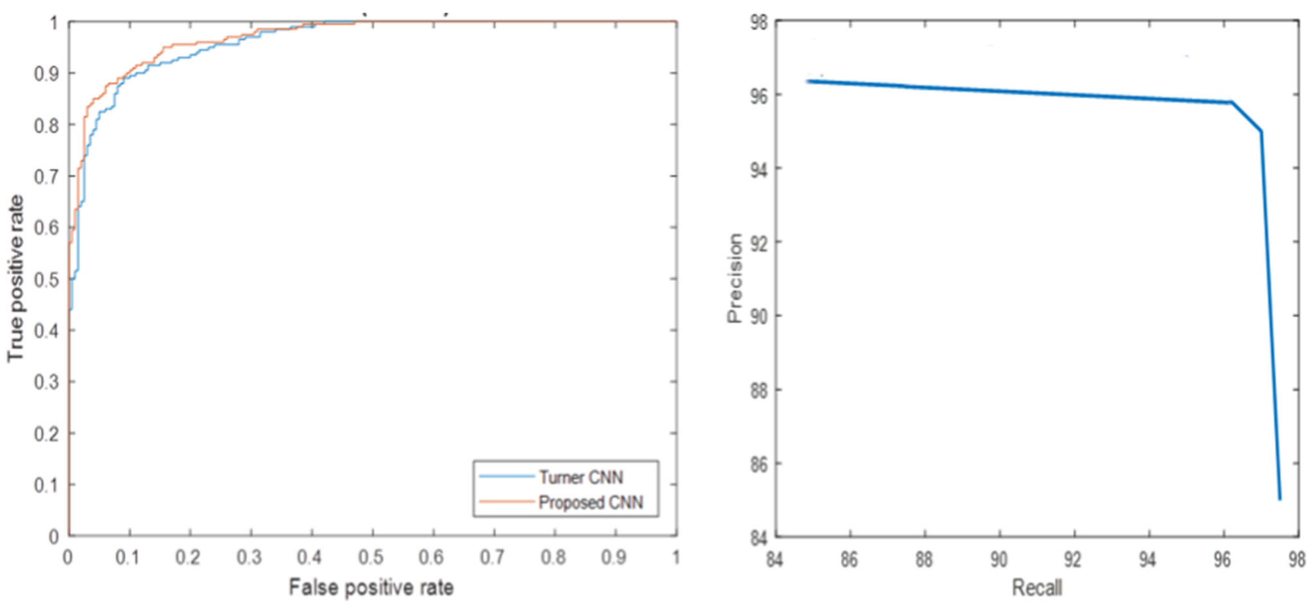

Fig. 10 ROC and precision recall curves for PS, S and NS cases

Table 10 Comparison between the proposed approaches and the other existing methods in terms of accuracy using the CHB-MIT dataset

Authors	Technique	Dataset	Classes	Accuracy
Shoeb [25]	SVM	CHB-MIT	NS-S	96
Sedik et al. [32]	SIFT, digital filters, and threshold classifier	6 patients from CHB-MIT	NS-S	99.16
			PS-S	96.24
Emara et al. [33]	FFT and ANN	CHB-MIT	NS-S	99.97
Emara et al. [34]	HHT and threshold classifier	CHB-MIT	PS-S	96.24
B. Bouaziz et al. [21]	CNN	CHB-MIT	NS-S	99.48
Rajaguru et al. [22]	MAE+EM-PCA	CHB-MIT	NS-S	93.78
Roy et al. [23]	ChronoNet	CHB-MIT	NS-S	86.57
Choi et al. [24]	3D-CNN+GRU	CHB-MIT	NS-S	89.4
Truong et al. [28]	Spectrograms+STFT	Freiburg higher-order statisticspital intra-cranial EEG	NS-S	81.4
		CHB-MIT		81.2
			S-PS	95.6
M. Zhou et al. [38]	CNN	CHB-MIT	NS-S	97.5
			NS-S-PS	93
			S-PS	96.7
		Freiburg	NS-S	95.4
			NS-S-PS	92.3
Kashif et al. [44]	LBP+LDA	14 patients from CHB-MIT	NS-S	99.6
			S-PS	97.66
Proposed approaches	Spectrogram+CNN	CHB-MIT	NS-S	95.59
			NS-S-PS	94.51
			S-PS	100
	HMS, sub-band energies, spectral entropies, higher-order statistics and SVM		NS-S	100

4 Conclusions

Two different approaches have been adopted for EEG signal classification in this paper. The first one depends on the HMS, spectral entropies, higher-order statistics and sub-band energies, while the second ones depends on a CNN model with spectrogram images. The models were evaluated on the CHB-MIT dataset. The obtained results for the ML-based model were 100% for accuracy, while the obtained results for the second CNN-based model were 97.66%, 95.59%, and 94.51% for seizure versus pre-seizure, non-seizure versus seizure, and non-seizure versus seizure versus pre-seizure classes, respectively. These results reveal that the proposed approaches have high accuracy in detecting seizures, and can be used for seizure detection in clinical settings. However, there are also some limitations to this research. One limitation is the small sample size of the CHB-MIT dataset, which may not be representative of the general population. Additionally, the models were only evaluated using EEG data, and it would be beneficial to evaluate the models using other types of neurological data as well. Future work could include expanding the dataset to include a larger and more diverse sample of individuals, evaluating the models using other types of neurological data, and exploring other ML techniques to improve the performance of the models. Additionally, it would be valuable to conduct a clinical trial to test the practical applicability of the proposed approaches in a real-world setting.

Funding This work has no funding.

Availability of data and material Raw data are available for all the experiments.

Code Availability Custom code.

Declarations

Ethics declarations We confirm that this work is original and has not been published elsewhere. It is not currently under consideration for publication elsewhere.

Conflicts of interest/Competing interests We have no conflict of interests to disclose.

References

1. Russ SA, Larson K, Halfon N (2012) A national profile of childhood epilepsy and seizure disorder. Pediatrics 129(2):256–264
2. Tomson T, Battino D, Bonizzoni E, Craig J, Lindhout D, Sabers A, Perucca E, Vajda F, Group ES (2011) Dose-dependent risk of malformations with antiepileptic drugs: an analysis of data from the eurap epilepsy and pregnancy registry. The Lancet Neurology 10(7):609–617
3. Cohen KB, Glass B, Greiner HM, Holland-Bouley K, Standridge S, Arya R, Faist R, Morita D, Mangano F, Connolly B et al (2016) Methodological issues in predicting pediatric epilepsy surgery candidates through natural language processing and machine learning. Biomedical informatics insights vol 8, pp BII–S38308
4. Yaffe R, Burns S, Gale J, Park H-J, Bulacio J, Gonzalez-Martinez J, Sarma SV (2012) Brain state evolution during seizure and under anesthesia: A network-based analysis of stereotaxic eeg activity in drug-resistant epilepsy patients. In 2012 Annual International Conference of the IEEE Engineering in Medicine and Biology Society, IEEE, pp 5158–5161
5. Yu P-N, Naiini SA, Heck CN, Liu CY, Song D, Berger TW (2016) A sparse laguerre-volterra autoregressive model for seizure prediction in temporal lobe epilepsy. In 2016 38th Annual International Conference of the IEEE Engineering in Medicine and Biology Society (EMBC), IEEE, pp 1664–1667
6. Mishra M, Jones B, Simonotto JD, Furman M, Norman WM, Liu Z, DeMarse TB, Carney PR, Ditto WL (2006) Pre-ictal entropy analysis of microwire data from an animal model of limbic epilepsy. In 2006 International Conference of the IEEE Engineering in Medicine and Biology Society, IEEE, pp 1605–1607
7. WHO (2017) Programmes and projects. http://www.who.int/mediacentre/factsheets/fs999/en/. Accessed 20 May 2021
8. Glauser T, Shinnar S, Gloss D, Alldredge B, Arya R, Bainbridge J, Bare M, Bleck T, Dodson WE, Garrity L et al (2016) Evidence-based guideline: treatment of convulsive status epilepticus in children and adults: report of the guideline committee of the american epilepsy society. Epilepsy currents 16(1):48–61
9. Pedram MZ, Shamloo A, Alasty A, Ghafar-Zadeh E (2015) Mri-guided epilepsy detection. In 2015 37th Annual International Conference of the IEEE Engineering in Medicine and Biology Society (EMBC), IEEE, pp 4001–4004
10. Simonotto JD, Myers SM, Furman MD, Norman WM, Liu Z, DeMarse TB, Carney PR, Ditto WL (2006) Coherence analysis over the latent period of epileptogenesis reveal that high-frequency communication is increased across hemispheres in an animal model of limbic epilepsy. In 2006 International Conference of the IEEE Engineering in Medicine and Biology Society, IEEE, pp 1154–1156
11. Taher F, Shoaib MR, Emara HM, Abdelwahab KM, El-Samie FEA, Haweel MT (2022) Efficient framework for brain tumor detection using different deep learning techniques. Frontiers in Public Health 10:959667
12. Shoaib MR, Elshamy MR, Taha TE, El-Fishawy AS, Abd El-Samie FE (2022) Efficient deep learning models for brain tumor detection with segmentation and data augmentation techniques. Concurrency and Computation: Practice and Experience 34(21):e7031
13. Shoaib MR, Emara HM, Elwekeil M, El-Shafai W, Taha TE, El-Fishawy AS, El-Rabaie E-SM, El-Samie E-SM (2022) Hybrid classification structures for automatic covid-19 detection. Journal of Ambient Intelligence and Humanized Computing 13(9):4477–4492
14. Emara HM, Shoaib MR, Elwekeil M, El-Shafai W, Taha TE, El-Fishawy AS, El-Rabaie E-SM, Alshebeili SA, Dessouky MI, Abd El-Samie FE (2022) Deep convolutional neural networks for covid-19 automatic diagnosis. Microscopy Research and Technique 84(11):2504–2516
15. Alam SS, Bhuiyan MIH (2013) Detection of seizure and epilepsy using higher order statistics in the emd domain. IEEE journal of biomedical and health informatics 17(2):312–318
16. Bizopoulos PA, Tsalikakis DG, Tzallas AT, Koutsouris DD, Fotiadis DI (2013) Eeg epileptic seizure detection using k-means clustering and marginal spectrum based on ensemble empirical mode decomposition. In 13th IEEE International Conference on BioInformatics and BioEngineering, IEEE,pp 1–4
17. Fu K, Qu J, Chai Y, Zou T (2015) Hilbert marginal spectrum analysis for automatic seizure detection in eeg signals. Biomedical Signal Processing and Control 18:179–185
18. Ibrahim FE, Emara HM, El-Shafai W, Elwekeil M, Rihan M, Eldokany IM, Taha TE, El-Fishawy AS, El-Rabaie E-SM, Abdellatef E et al (2022) Deep learning-based seizure detection and prediction from eeg signals. International Journal for Numerical Methods in Biomedical Engineering, p e3573
19. Riaz F, Hassan A, Rehman S, Niazi IK, Dremstrup K (2015) Emd-based temporal and spectral features for the classification of eeg signals using supervised learning. IEEE Transactions on Neural Systems and Rehabilitation Engineering 24(1):28–35
20. Hassan AR, Subasi A, Zhang Y (2019) Epilepsy seizure detection using complete ensemble empirical mode decomposition with adaptive noise. Knowledge-Based Systems, p 105333
21. Bouaziz B, Chaari L, Batatia H, Quintero-Rincón A (2019) Epileptic seizure detection using a convolutional neural network. In Digital Health Approach for Predictive, Preventive, Personalised and Participatory Medicine, Springer, pp 79–86
22. Rajaguru H, Prabhakar SK (2018) Multilayer autoencoders and em-pca with genetic algorithm for epilepsy classification from eeg. In 2018 Second International Conference on Electronics, Communication and Aerospace Technology (ICECA), IEEE, pp 353–358
23. Roy S, Kiral-Kornek I, Harrer S (2019) Chrononet: a deep recurrent neural network for abnormal eeg identification. In Conference on Artificial Intelligence in Medicine in Europe, Springer, pp 47–56
24. Choi G, Park C, Kim J, Cho K, Kim T-J, Bae H, Min K, Jung K-Y, Chong J (2019) A novel multi-scale 3d cnn with deep neural network for epileptic seizure detection. In 2019 IEEE International Conference on Consumer Electronics (ICCE), IEEE, pp 1–2
25. Shoeb AH (2009) Application of machine learning to epileptic seizure onset detection and treatment. Ph.D. dissertation, Massachusetts Institute of Technology
26. Thodoroff P, Pineau J, Lim A (2016) Learning robust features using deep learning for automatic seizure detection. In Machine Learning for Healthcare Conference, Springer, pp 178–190

27. Cura OK, Atli SK, Türe HS, Akan A (2020) Epileptic seizure classifications using empirical mode decomposition and its derivative. BioMedical Engineering OnLine 19(1):1–22
28. Truong ND, Nguyen AD, Kuhlmann L, Bonyadi MR, Yang J, Ippolito S, Kavehei O (2018) Convolutional neural networks for seizure prediction using intracranial and scalp electroencephalogram. Neural Networks 105:104–111
29. Ozdemir N, Yildirim E (2014) Patient specific seizure prediction system using hilbert spectrum and bayesian networks classifiers. Computational and mathematical methods in medicine, vol 2014
30. Consul S, Morshed BI, Kozma R (2013) Hardware efficient seizure prediction algorithm. In Nanosensors, Biosensors, and Info-Tech Sensors and Systems 2013 International Society for Optics and Photonics, vol 8691, p 86911J
31. Chu H, Chung CK, Jeong W, Cho K-H (2017) Predicting epileptic seizures from scalp eeg based on attractor state analysis. Computer methods and programs in biomedicine 143:75–87
32. Sedik A, Emara HM, Hamad A, Shahin EM, El-Hag NA, Khalil A, Ibrahim F, Elsherbeny ZM, Elreefy M, Zahran O et al (2019) Efficient anomaly detection from medical signals and images. International Journal of Speech Technology 22(3):739–767
33. Emara HM, Elwekeil M, Taha TE, El-Fishawy AS, El-Rabaie E-SM, El-Shafai W, El Banby GM, Alotaiby T, Alshebeili SA, El-Samie A et al (2021) Efficient frameworks for eeg epileptic seizure detection and prediction. Annals of Data Science, pp 1–36
34. Emara HM, Elwekeil M, Taha TE, El-Fishawy AS, El-Rabaie E-SM, Alotaiby T, Alshebeili SA, El-Samie A, Fathi E (2021) Hilbert transform and statistical analysis for channel selection and epileptic seizure prediction. Wireless Personal Communications 116(4):3371–3395
35. Yoo J, Yan L, El-Damak D, Altaf MAB, Shoeb AH, Chandrakasan AP (2012) An 8-channel scalable eeg acquisition soc with patient-specific seizure classification and recording processor. IEEE journal of solid-state circuits 48(1):214–228
36. Rana P, Lipor J, Lee H, Van Drongelen W, Kohrman MH, Van Veen B (2012) Seizure detection using the phase-slope index and multichannel ecog. IEEE Transactions on Biomedical Engineering 59(4):1125–1134
37. Khamis H, Mohamed A, Simpson S (2013) Frequency-moment signatures: a method for automated seizure detection from scalp eeg. Clinical Neurophysiology 124(12):2317–2327
38. Zhou W, Liu Y, Yuan Q, Li X (2013) Epileptic seizure detection using lacunarity and bayesian linear discriminant analysis in intracranial eeg. IEEE Transactions on Biomedical Engineering 60(12):3375–3381
39. Liu Y, Zhou W, Yuan Q, Chen S (2012) Automatic seizure detection using wavelet transform and svm in long-term intracranial eeg. IEEE transactions on neural systems and rehabilitation engineering 20(6):749–755
40. Vidyaratne L, Glandon A, Alam M, Iftekharuddin KM (2016) Deep recurrent neural network for seizure detection. In 2016 International Joint Conference on Neural Networks (IJCNN), IEEE, pp 1202–1207
41. Shoeb AH, Guttag JV (2010) Application of machine learning to epileptic seizure detection. In ICML
42. Pramod S, Page A, Mohsenin T, Oates T (2014) Detecting epileptic seizures from eeg data using neural networks. arXiv preprint arXiv:1412.6502
43. Turner J, Page A, Mohsenin T, Oates T (2014) Deep belief networks used on high resolution multichannel electroencephalography data for seizure detection. In 2014 AAAI Spring Symposium Series
44. Khan KA, Shanir P, Khan YU, Farooq O (2020) A hybrid local binary pattern and wavelets based approach for eeg classification for diagnosing epilepsy. Expert Systems with Applications 140:112895
45. Orosco L, Correa AG, Diez P, Laciar E (2016) Patient non-specific algorithm for seizures detection in scalp eeg. Computers in biology and medicine 71:128–134
46. Al Safi A, Beyer C, Unnikrishnan V, Spiliopoulou M (2020) Multivariate time series as images: Imputation using convolutional denoising autoencoder. In International Symposium on Intelligent Data Analysis, Springer, pp 1–13
47. Wang Z, Oates T (2015) Encoding time series as images for visual inspection and classification using tiled convolutional neural networks. In Workshops at the twenty-ninth AAAI conference on artificial intelligence
48. Barra S, Carta SM, Corriga A, Podda AS, Recupero DR (2020) Deep learning and time series-to-image encoding for financial forecasting. IEEE/CAA Journal of Automatica Sinica 7(3):683–692
49. Kukker A, Sharma R (2021) A genetic algorithm assisted fuzzy q-learning epileptic seizure classifier. Computers & Electrical Engineering 92:107154
50. Jareda MK, Sharma R, Kukker A (2019) Eeg signal based seizure classification using wavelet transform. In 2019 International Conference on Computing, Power and Communication Technologies (GUCON), IEEE, pp 537–539
51. PhysioNet (2000) CHB-MIT Scalp EEG Database. https://www.physionet.org/pn6/chbmit/. Accessed 1 Jan 2017
52. Hassan AR (2015) A comparative study of various classifiers for automated sleep apnea screening based on single-lead electrocardiogram. In 2015 International Conference on Electrical & Electronic Engineering (ICEEE), IEEE, pp 45–48
53. Hassan AR, Bhuiyan MIH (2016) Computer-aided sleep staging using complete ensemble empirical mode decomposition with adaptive noise and bootstrap aggregating. Biomedical Signal Processing and Control 24:1–10
54. Zamanian H, Farsi H (2018) A new feature extraction method to improve emotion detection using eeg signals. ELCVIA Electronic Letters on Computer Vision and Image Analysis 17(1):29–44
55. Wang H, Ji Y (2018) A revised hilbert-huang transform and its application to fault diagnosis in a rotor system. Sensors 18(12):4329
56. Toh AM, Togneri R, Nordholm S (2005) Spectral entropy as speech features for speech recognition. Proceedings of PEECS 1:92
57. Kannathal N, Choo ML, Acharya UR, Sadasivan P (2005) Entropies for detection of epilepsy in eeg. Computer methods and programs in biomedicine 80(3):187–194
58. Lehman A (1964) A solution of the shannon switching game. Journal of the Society for Industrial and Applied Mathematics 12(4):687–725
59. Rényi A, Vekerdi L (1970) Calcul des probabilités. North-Holland Publishing Company, vol 10
60. Tsallis C (1988) Possible generalization of boltzmann-gibbs statistics. Journal of statistical physics 52(1–2):479–487
61. Bajaj V, Pachori RB (2013) Automatic classification of sleep stages based on the time-frequency image of eeg signals. Computer methods and programs in biomedicine 112(3):320–328
62. Omerhodzic I, Avdakovic S, Nuhanovic A, Dizdarevic K (2013) Energy distribution of eeg signals: Eeg signal wavelet-neural network classifier. arXiv preprint arXiv:1307.7897
63. Huang NE, Shen Z, Long SR, Wu MC, Shih HH, Zheng Q, Yen N-C, Tung CC, Liu HH (1998) The empirical mode decomposition and the hilbert spectrum for nonlinear and non-stationary time series analysis. Proceedings of the Royal Society of London. Series A: mathematical, physical and engineering sciences 454(1971):903–995
64. Khoshnevis SA, Sankar R (2019) Applications of higher order statistics in electroencephalography signal processing: a comprehensive survey. IEEE Reviews in biomedical engineering 13:169–183

65. Šimundić A-M (2008) Measures of diagnostic accuracy: basic definitions. Medical and biological sciences 22(4):61–65
66. Azar AT, El-Said SA (2014) Performance analysis of support vector machines classifiers in breast cancer mammography recognition. Neural Computing and Applications 24(5):1163–1177
67. Salam MT, Sawan M, Nguyen DK (2010) Low-power implantable device for onset detection and subsequent treatment of epileptic seizures: A review. Journal of Healthcare Engineering 1(2):169–184

Essam Abdellatef received the Master degree in Electronics and Communications Engineering from the Faculty of Engineering, Mansoura University, Egypt in 2015. Also, he received the PhD degree in Electronics and Communications Engineering from the Faculty of Electronic Engineering, Menoufia University, Egypt by 2019. He is now an assistant professor at the electronics and communications engineering department, Delta Higher Institute for Engineering and Technology-Egypt. His main research area includes Deep Learning applications, 3D object reconstruction and image encryption.

Heba M. Emara received the B.Sc and M.Sc degrees from Menoufia University, Menouf, Egypt, in 2002, and 2019, respectively. Her current research interests include image processing, medical signal and image processing, digital communications, Internet of Things, Medical Diagnoses Applications, FPGA Implementations for Signal Processing Algorithms and Communication Systems, Machine learning, and Deep Learning Applications.

Mohamed Reda Shoaib received the Master degree in Electronics and Communications Engineering from the Faculty of Engineering, Menoufia University, Egypt by 2022. He is now a Machine learning and Data Science Engineer at the shgardi Company. His main research area includes Artificial intelligence, Machine learning, DL, Computer vision, Data science applications, Biomedical engineering and Health care applications.

Fatma El-Sayed Ali Ibrahim received the B. Sc. in Electronics and Electrical Communication Engineering from the Faculty of Electronic Engineering, Menoufia University, Egypt in 2001. She received the M. Sc. in Electronics in the field of Planning and Communications System Engineering from the Faculty of Electronic Engineering, Menoufia University, Egypt in 2009. She received the Master of Business Administration (MBA) from ESLSCA Business School in cooperation with Université Française d'Egypte, Egypt in 2017. Her main research areas include image processing, medical signal and image processing, and DL applications.

Mohamed Elwekeil received the B.Sc. in Electronics and Electrical Communications Engineering from the Faculty of Electronic Engineering, Menoufia University, Egypt in 2007. He received the M.Sc. and the PhD in Electronics and Communications Engineering from Egypt-Japan University of Science and Technology (E-JUST), Alexandria, Egypt in 2013 and 2016, respectively. He was a teaching assistant in the department of Electronics and Electrical Communications Engineering, Faculty of Electronic Engineering, Menoufia University, Egypt in the period from December 2007 to November 2016. In December 2016, he has been promoted to a lecturer (assistant professor) position in the same department. In the period from April 2014 till March 2015, he was a research intern at Alcatel-Lucent Bell N.V. (now NOKIA), Antwerp, Belgium, where he was working on WiFi optimization project. In October 2015, he has joined Kyushu University, Fukuoka, Japan, as a special research student for a period of 9 months. In the period from April 2018 to March 2020, he was with the College of Information Engineering, Shenzhen University, Shenzhen, China, where he was working as a post-doctoral researcher. His research interests include radio resource management for wireless networks, spatial modulation, and signal processing for communications.

Walid El-Shafai was born in Alexandria, Egypt. He received the B.Sc. degree (Hons.) in Electronics and Electrical Communication Engineering from Faculty of Electronic Engineering (FEE), Menoufia University, Menouf, Egypt in 2008, M.Sc. degree from Egypt- Japan University of Science and Technology (E-JUST) in 2012, and a Ph.D. degree from the Faculty of Electronic Engineering, Menoufia University, Menouf, Egypt in 2019. He is currently working as a Lecturer and an Assistant professor in ECE Dept. FEE, Menoufia University. Since January 2021, he joined as a Postdoctoral Research Fellow at the Security Engineering Lab (SEL) at Prince Sultan University (PSU). His research interests are in the areas of Wireless Mobile and Multimedia Communications Systems, Image and Video Signal Processing, Efficient 2D Video, Cognitive Cryptography, Medical Image Processing, Speech Processing, Security Algorithms, Software Defined Networks, Internet of Things, Medical Diagnoses Applications, FPGA Implementations for Signal Processing Algorithms and Communication Systems, Cancellable Biometrics and Pattern Recognition, Modulation Identification and Classification, Image and Video Super-Resolution and Denoising, Cybersecurity Applications, Deep Learning in Signal Processing and Communication Systems Applications. Walid has several publications in the above research areas in several reputable international and local Journals and conferences. Also, he serves as a reviewer in several International Journals.

Taha E. Taha was born in Tanta, Egypt, on October 11, 1946. He received the B.Sc. degree (with distinction) in communications engineering from Menoufia University, Egypt, in June 1969, the M.Sc. degree in communication engineering from Helwan University, Egypt, in April 1978, and the Ph.D. degree (very honorable) in electronic engineering from the National Polytechnic Institute, Toulouse, France, in June 1985. From September 1969 to July 1978, he was a demonstrator. In July 1978, he was an Assistant Lecturer. In November 1985, he was a Lecturer. In February 1990, he was an Assistant Professor. In September 1995, he was named Professor at the Faculty of Electronic Engineering, Menoufia University, Communications Department. He was appointed as Vice Dean from February 2002 to October 2005, and Head of the Communications Department, from November 2005 to July 2007. At present, he is a Professor Emeritus at the same department. His main research interests are surface acoustic wave devices, optical devices, superconductor devices, medical applications of ultrasound, medical imaging, and bio-informatics.

Adel S. El-Fishawy received the B.Sc. in electronics and communications engineering, Menoufia University, in 1974 and the M.Sc degree from Cairo University, Egypt, in 1982. He received the Ph.D degree in signals and systems from Drexel University, ECE Dept., Phila., PA, USA, 1990. He is working as a Professor Emeritus with the Department of Electronics and Electrical Communications Engineering, Faculty of Electronic Engineering, Menoufia University, Egypt. His areas of interest are electronics, modeling and simulations, digital communications, signal, speech, biomedical image processing, and digital communications.

El-Sayed M. El-Rabaie (SM'92) was born in Sires Elian, Egypt, in 1953. He received the B.Sc. degree (with honors) in radio communications from Tanta University, Tanta, Egypt, in 1976, the M.Sc. degree in communication systems from Menoufia University, Menouf, Egypt, in 1981, and the Ph.D. degree in microwave device engineering from Queen's University of Belfast, Belfast, U.K., in 1986. In his doctoral research, he constructed a Computer-Aided Design (CAD) package used in nonlinear circuit simulations based on the harmonic balance techniques. Up to February 1989, he was a Postdoctoral Fellow with the Department of Electronic Engineering, Queen's University of Belfast. He was invited as a Research Fellow in the College of Engineering and Technology, Northern Arizona University, Flagstaff, in 1992 and as a Visiting Professor at Ecole Poly technique de Montreal, Montreal, QC, Canada, in 1994. He has authored and co-authored more than 300 papers and nineteen textbooks. He was given several awards (Salah Amer Award of Electronics in 1993, The Best Researcher on (CAD) from Menoufia University in 1995). He acts as a reviewer and member of the editorial board for several scientific journals. He has participated in translating the first part of the Arabic Encyclopedia. Professor El-Rabaie was the Head of the Electronics and Communication Engineering Department, Faculty of Electronic Engineering, Menoufia University, and after that the Vice Dean of Postgraduate Studies and Research at the same Faculty. Prof. El-Rabaie is involved now in different research areas including CAD of nonlinear.

Ibrahim Eldokany is a Professor Emeritus at the Faculty of Electronic Engineering. He had the B.Sc. in Communications Engineering, Mounofia University, Egypt, 1963. From 1968 to 1972, he had a governmental scholarship for Ph.D. in Germany. He had the Ph.D. degree in microelectronics in 1972, Chimnitz University, Germany. His research interests include microelectronics technology, adaptive filters, adaptive equalizers, wireless communications, modulation systems, spread spectrum techniques, switched capacitor circuits, signal processing for communications, medical signal and image processing, forensic analysis, mechatronics, integrated optics, radiation effect on optical fibers, power line communications, multi-user detection systems, and acoustics. He died in 2022.

Fathi E. Abd El-Samie received the B.Sc. (Hons.), M.Sc., and Ph.D. degrees from Menoufia University, Menouf, Egypt, in 1998, 2001, and 2005, respectively. Since 2005, he has been a Teaching Staff Member with the Department of Electronics and Electrical Communications, Faculty of Electronic Engineering, Menoufia University. He worked as a researcher at KACST-TIC in Radio Frequency and Photonics for the e-Society (RFTONICs) from 2013 to 2015. His current research interests include image processing, multimedia communications, medical signal and image processing, optical signal processing, and digital communications. He was a recipient of the Most Cited Paper Award from the Digital Signal Processing journal in 2008.

Authors and Affiliations

Essam Abdellatef[1] · **Heba M. Emara**[2] · **Mohamed R. Shoaib**[3] · **Fatma E. Ibrahim**[2] · **Mohamed Elwekeil**[2] · **Walid El-Shafai**[2,4] · **Taha E. Taha**[2] · **Adel S. El-Fishawy**[2] · **El-Sayed M. El-Rabaie**[2] · **Ibrahim M. Eldokany**[2] · **Fathi E. Abd El-Samie**[2,5]

Essam Abdellatef
essam_abdellatef@yahoo.com

Heba M. Emara
hebam9909@gmail.com

Mohamed R. Shoaib
MOHAMEDR003@e.ntu.edu.sg

Fatma E. Ibrahim
eng.fatmaelsayed@gmail.com

Mohamed Elwekeil
mohamed.elwekeil@el-eng.menofia.edu.eg

Taha E. Taha
taha117@hotmail.com

Adel S. El-Fishawy
aelfishawy@hotmail.com

El-Sayed M. El-Rabaie
Srabie1@yahoo.com

Ibrahim M. Eldokany
ibdok@yahoo.com

Fathi E. Abd El-Samie
fathi_sayed@yahoo.com

1 Department of Electronics and Communications, Delta Higher Institute for Engineering and Technology (DHIET), 35511 Mansoura, Egypt

2 Faculty of Electronic Engineering, Menoufia University, 32952 Menouf, Egypt

3 School of Computer Science and Engineering, Nanyang Technological University, Singapore, Singapore

4 Security Engineering Laboratory, Department of Computer Science College of Engineering, Prince Sultan University, Riyadh 11586, Saudi Arabia

5 Department of Information Technology, College of Computer and Information Sciences, Princess Nourah Bint Abdulrahman University, P.O. Box 84428, 11671 Riyadh, Saudi Arabia